Chapter 4:   Steering and Orbit Correction

4.1   *Motivation*

Precise control of centroid orbit is necessary for good beam recirculation, with low losses due to large centroid deviations. This allows for observation of beam losses due to more complex effects, such as resonant excitation of particle and/or beam envelope amplitudes, as well as longitudinal losses. The proposed quasi-integrable nonlinear optics experiment has, as its lowest-order, most straightforward diagnostic, a characterization of resonantly driven beam losses with and without nonlinear damping. Therefore, a reduction of transverse scraping losses is imperative for observation of these likely slower loss rates. Additionally, the nonlinear optics experiments require a low-current, high-emittance $60\mu A$ beam. A large emittance beam corresponds to a large cross-section beam in configuration space, which places a more stringent requirement on steering tolerances.

In an ideal linear accelerator, there exists a "reference trajectory," which describes the path of an ideal particle. This trajectory is typically centered within the focusing quadrupoles and the beam pipe. A beam with imperfect injection conditions will oscillate about the ideal trajectory. In this section, we define "first-turn orbit" to mean the measured or simulated centroid trajectory on the first

turn. "Closed orbit" refers to the orbit about which the trajectory oscillates. This is also referred to as the "equilibrium orbit." Ideally this orbit is centered in the quadrupoles, but due to background field, alignment errors and number of available correctors, it is only possible to minimize orbit deviation from quadrupole centers.

In general, for straightforward operation of UMER, lowest-possible deviation of beam centroid from quadrupole centers in multi-turn operation is desireable, for the smallest coupling between focusing strength and closed orbit deviation. As seen in Section **??**, the dynamic aperture of the quasi-integrable octupole lattice suffers greatly for orbit distortions, and it is desirable to minimize centroid offset from octupole centers in the octupole insert.

4.2   Considerations for low-ridgidity electron beam

In typical high-energy accelerating or storage rings (for which steering algorithms are well-developed), the beam travels in straight lines between steering elements (dipoles or off-centered quadrupoles), effectively tracing out an N-sided polygon where N is the number of dipoles. Steering in UMER is complicated by the fact that at low-energies, the beam is significantly bent by background, ambient fields. For a 10 keV electron beam, rigidity $B\rho = \frac{p}{q}$ is 338.859 G-cm. The required integrated field to bend the beam 10° is 59.154 G-cm. Given an average ambient vertical field of ≈ 400 mG, per 32 cm cell, the integrated field is $32 * 0.400 = 12.8$ G-cm. Therefore, approximately 22% of the total horizontal bending in the ring is due to the ambient vertical fields. The ambient horizontal field is weaker, on
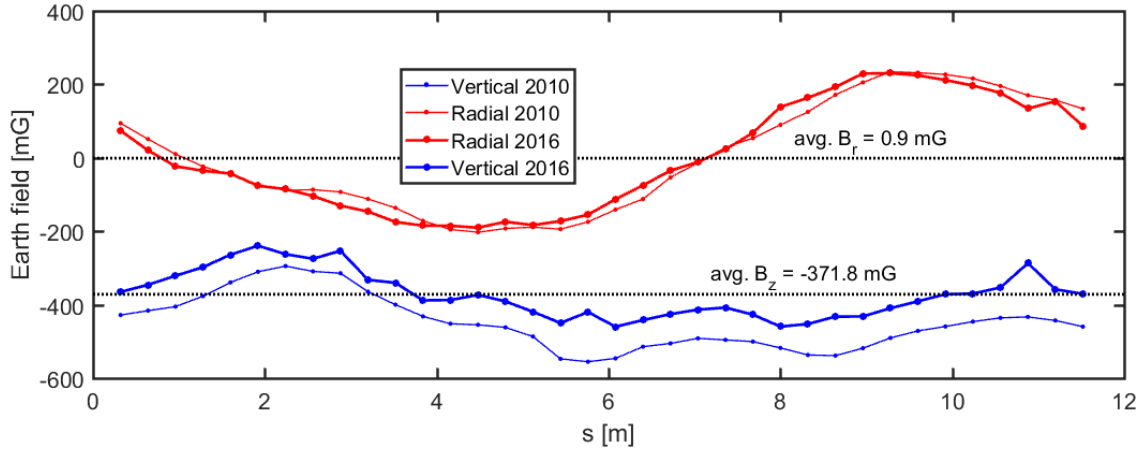
Fig. 4.1: Ambient fields measured at UMER dipoles, from Dave Sutter measurements 6/1/2010 and 7/22/2016.

average < 1 mG, which gives only a small orbit distortion (requiring only a small correction) from turn-to-turn. However, local closed orbit distortions due to the horizontal fields can be large (up to ≈ 200 mG), and large vertical corrections are necessary to minimize deviation from quadrupole centers. Measured ambient field data can be seen in Figs. 4.1 and 4.2.

Because the beam is immersed in a bending field, in the perfectly aligned case a beam orbit that is centered in the quadrupoles is required to be displaced in the BPMs, as in Fig. 4.3. Simple calculations with a constant background field show that we expect the ideal orbit to be radially displaced by [todo:]. However, in the case of azimuthally-varying ambient fields and displacements up to several millimeters, we expect larger displacements of the "best-possible" orbit.

Steering in the ring is controlled by 36 horizontal bending dipoles, which determine the shape of the horizontal closed orbit, and which can be independently
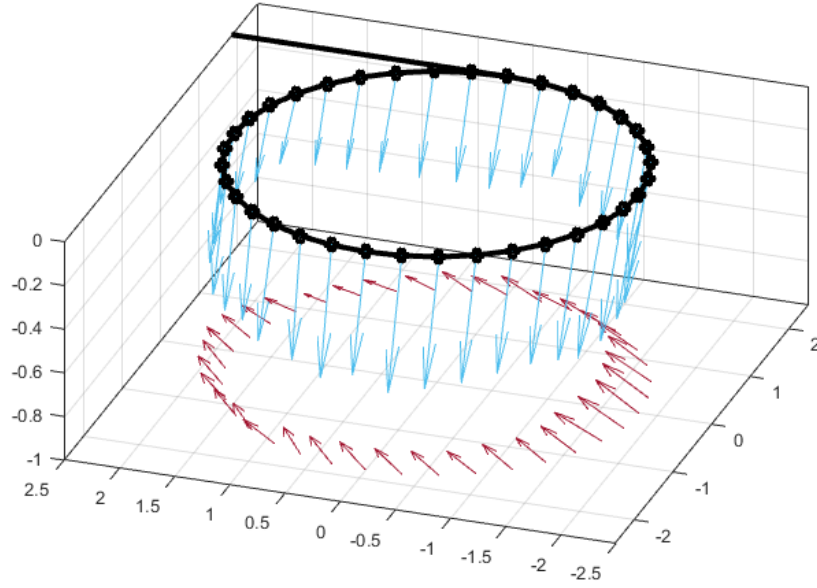
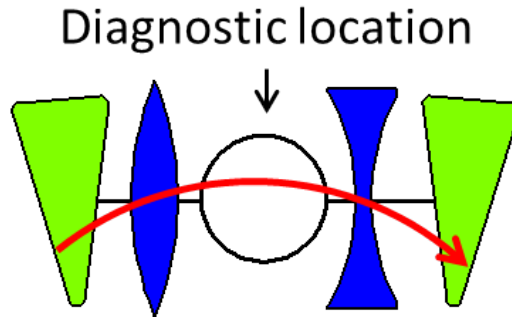*Fig. 4.2:* Ambient field data vectors, including xy projection. x,y units are meters, z-axis is milli-Gauss.

Fig. 4.3: Diagram of beam position in diagnostic (BPM) for an orbit that is horizontally centered in the quadrupoles.

adjusted to optimizie the orbit. This is different from the typical case of a larger ring, which uses fixed dipoles and adjustable corrector magnets. There is 1 independent horizontal dipole every 2 quadrupoles. Vertical correction is made with 18 printed circuit corrector magnets located at pipe flanges, which are named "RSV" magnets. There is 1 RSV corrector every 4 quadrupoles. Additional vertical correctors have been added and proposed, as described in Section **??**. Steering near injection is controlled by 6 vertical and horizontal corrector magnets in the injection line, in the "SDH" and "SDV" families. Additionally, there are two correctors (one horizontal and one vertical) in the ring near the intersection of the injection pipe (the "Y-section"), named "SDR6H" and "SDR6V."

4.3   UMER Steering Magnets

Tab. 4.1: UMER Steering magnet strengths

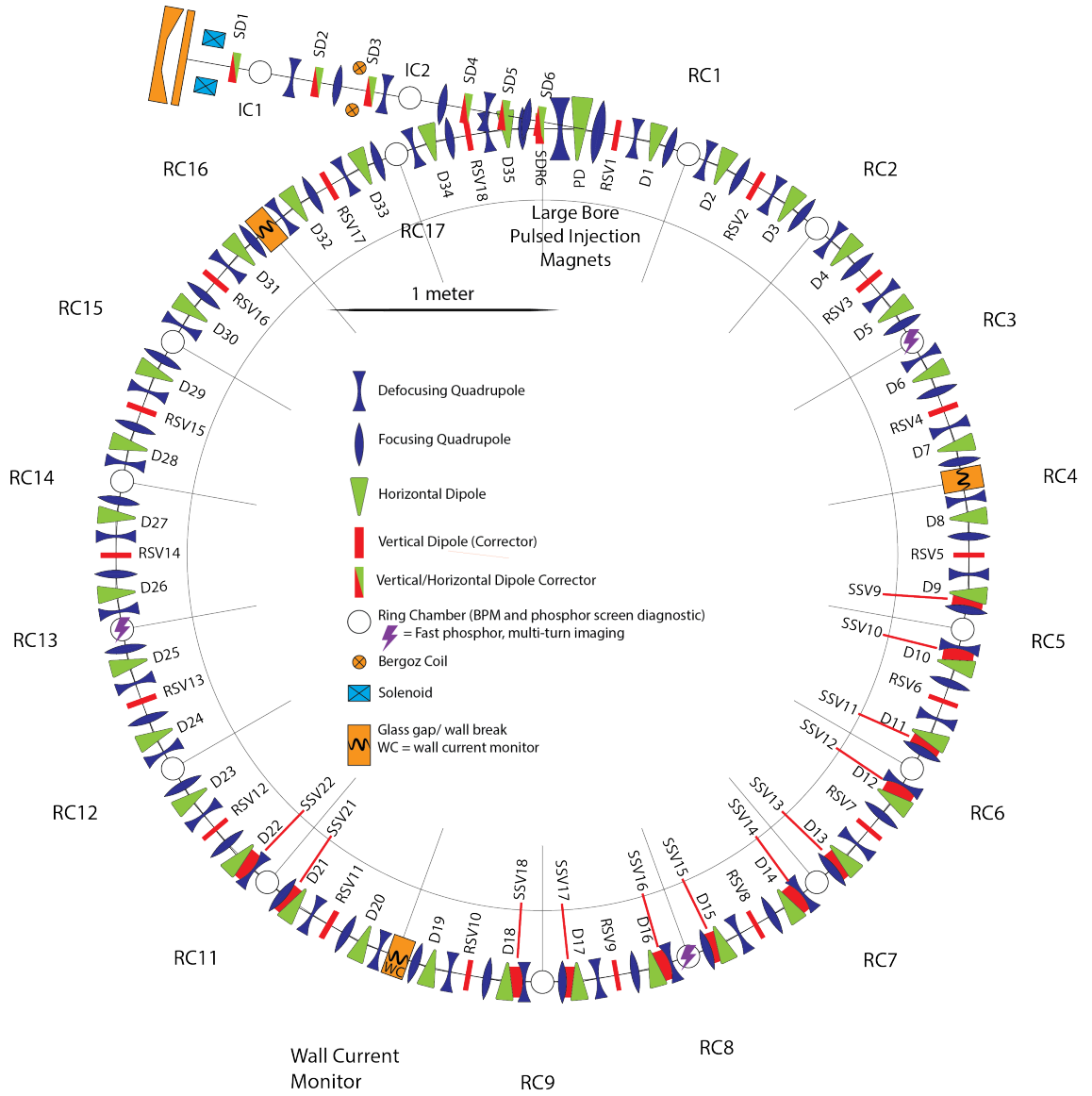| Magnet Name	length [cm]	radius [cm]	Integ. Field / A [G-cm/A]	strength [^{o}/A]
BD	4.44	2.87	19.917	3.37
PD	4.40	4.40	1.913	0.32
RSV	3.80	5.75	3.886	0.66
SD	2.37	4.73	3.317	0.56
SSV	1.54	2.79	3.627	0.61

Fig. 4.4: UMER Diagram with all steerers labelled. SSV family is discussed in Section 4.8

4.4   Prior Approach

An alternative approach to steering was developed using a steering procedure with local corrections to ensure the equilibrium orbit is centered (or as close to centered as possible) in the quadrupoles. This is unique from the response matrix method, in which a global correction is calculated that aims to center the equilibrium orbit at the 14 BPM locations. The steering algorithm is a methodical, "front to back" approach that first minimizes the position of the beam in the quadrupoles on the first turn then minimizes orbit deviations in subsequent turns. This algorithm should result in smaller local orbit excursions from quadrupole centers, since it utilizes 36 position data points at quadrupole locations for the first turn orbit as opposed to 14 at the BPMs. This is proposed as a alternative to the response matrix steering algorithm [1], and may be more useful for applications where orbit centering in the quadrupoles is essential.

The remainder of this chapter describes the tools and algorithmic approach to centering the first turn orbit in the quadrupole centers. First I describe the quad-as-BPM procedure for measuring first-turn centroid position at the quadrupoles (Section 4.5). Then I summarize the application of various algorithms to set horizontal and vertical steerers in Section **??**, including theoretical "best-case" orbit excursions and proposed vertical steering upgrades to meet the dynamic aperture requirements for the nonlinear optics experiments. This includes first-turn data taken during ring steering tests. Section 4.7 lays out a sample steering procedure, including injection and multi-turn optimization routines.
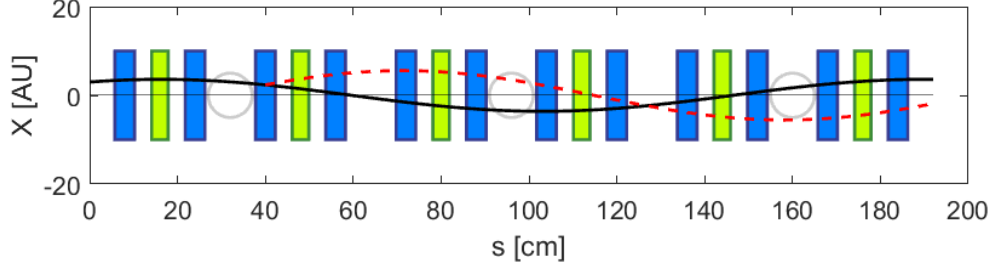
Fig. 4.5: Diagram of UMER beamline, with quadrupoles (blue), dipoles (green) and BPMs (circles). Black curve is possible centroid trajectory, dashed-red curve is perturbed centroid due to change in quadrupole strength at 40 cm. Phase advance per cell (32 cm) is 66.4^o.

4.5   Quadrupole as BPM technique

First-turn position data is extrapolated from quadrupole response data, also called "quad as BPM" or "virtual BPM." A beam that is off-centered in a quadrupole will experience a dipole force acting on the centroid motion as well as a quadrupole focusing force that acts on the beam envelope, as shown in Fig. 4.5. The strength of the dipole kick will depend on the position of the centroid in the quadrupole as well as strength of the quadrupole. Variation of the quadrupole strength will cause variation of the centroid as detected on a downstream BPM. Knowledge of the centroid transformation between quadrupole and BPM allows reconstruction of the beam position.

In a lattice with low phase advance per cell (such as UMER, with 66.4^o and 67.5^o in the x,y planes), the particle motion is approximately sinusoidal, described by:

$$x(s) = A_1 \cos \frac{\sigma}{L} s + A_2 \sin \frac{\sigma}{L} s \tag{4.1}$$

The derivative of this motion is

$$x'(s) = \frac{dX}{ds} = -A_1 \frac{\sigma}{L} \sin \frac{\sigma}{L} s + A_2 \frac{\sigma}{L} \cos \frac{\sigma}{L} s \tag{4.2}$$

Generally, the centroid is not confined to the reference orbit (the orbit that goes through the center of every quad), so the equilibrium centroid orbit oscillates with a frequency of $2\pi \times \nu$, with amplitudes A. Now, let's consider an orbit that has been perturbed, due to changing the strength of a single quad. We treat the quadrupole as "thin," an appropriate simplification when phase advance is low. Using the analog of thin lens optics in the paraxial approximation, $\Delta x' \approx tan\Delta x' = \frac{x_Q}{f}$ where x_Q is the centroid offset in the quad and f is the focal length. For a thin quadrupole, $\frac{1}{f} = \frac{G}{B\rho}$ for integrated gradient G and magnetic rigidity $B\rho$. For UMER ring quadrupoles, $G = 13.50I$ [Gauss/A] and for 10 keV electrons, $B\rho = 338.85$ G-cm.

Consider a perturbed orbit $\tilde{x}(s) = x(s) + \delta x(s)$, where $s = 0$ is the perturbed quad location. The initial conditions are $\tilde{x}(0) = x(0)$ and $\tilde{x}'(0) = x'(0) + \Delta x'_Q$ where $\Delta x'_Q = x(\frac{G\Delta I}{B\rho})$ is the change in angle due to perturbation on the quad. Letting $\delta x(s) = B_1 \cos \sigma s/L + B_2 \sin \sigma s/L$ and applying these initial conditions, we find $B_1 = 0$, $B_2 = x_Q L/\sigma \times G\Delta I/B\rho$ and the perturbed orbit is:

$$\tilde{x}(s) = x(s) + x_Q \frac{L}{\sigma} \frac{G\Delta I}{B\rho} \sin \frac{\sigma}{L} s \tag{4.3}$$

With variation of the quadrupole strength, we find the dependence of the

centroid position in a downstream BPM is linear in the position in the quadrupole, x_Q:

$$\frac{d\tilde{x}(s_{BPM})}{d\Delta I} = x_Q \frac{L}{\sigma} \frac{G}{B\rho} \sin \frac{\sigma}{L} s_{BPM} \qquad (4.4)$$

In the approach described here, we recover the first-turn position in the quadrupoles by measuring the slope $\frac{d\tilde{x}(s_{BPM})}{d\Delta I}$. A model of the ring using the VRUMER beam tracking code is used to calculate the constant $\frac{L}{\sigma} \frac{G}{B\rho} \sin \frac{\sigma}{L} s_{BPM}$, the result is a measurement of x_Q. This is an essentially identical method to that described by Kamal Poor Rezaei [2], with the main difference being the use of the VRUMER beam tracking code to calibrate position, rather than a transfer matrix calculation.

VRUMER, described in detail in Appendix [TBD], is a simple orbit integrator written in Matlab, originally developed by Irving Haber to model transverse beam centroid behavior and test UMER-specific steering algorithms. The model used here includes the measured background earth field, applied as a continuously acting, lab-frame-position dependent force based on linear interpolation between measurement points at the 36 dipoles. This model does not include centroid kicks as a result of magnet fringe fields or the steering effect of the offset YQ magnet, although the framework can support these refinements.

At an operating point of 1.826 A, the UMER 6 mA beam has $\nu_x = 6.636$, $\nu_y = 6.752$ [3]. This corresponds to betatron wavelengths $\lambda_x = 1.736$ m, $\lambda_y = 1.706$ m. In the VRUMER simulation, horizontal and vertical tunes are equal (no edge focusing), $\nu = 6.293$, equivalently $\lambda = 1.83$ m. In this case, quadrupole strength

parameters were set according to standard hard-edged approximation for the UMER quadrupoles: length= 4.475 cm, peak strength $g = 3.609$ G/cm, hard-edge factor $f = 0.8354$.

4.5.1 Systematic Error in Quad-as-BPM Calibration

The previous section begs the question, what is the amount of systematic error introduced by differences between reality and the model used for calibration (in this case, VRUMER). Most notably, bare tune in the model and measured tune differ by $\Delta\nu_x = 0.340$ horizontally, $\Delta\nu_y = 0.459$ vertically. It is covenient to define phase advance per cell, $\sigma = \frac{2\pi\nu}{36}$. Additionally, there are measurement errors included in the measurement of position with BPM.

Examining the formula for x_Q from Eq. 4.4 above, re-written here as:

$$x_Q = \frac{\sigma}{L}\frac{d\tilde{x}_{BPM}}{d\Delta I}\sin^{-1}\frac{\sigma}{L}s_{BPM} \qquad (4.5)$$

Applying error analysis and assuming no significant error is introduced by our choice of L, G, $B\rho$, or s_{BPM} in the model, we find the position error to be dependent on errors in the measured slope m, σ_m, and the systematic error of the model phase advance σ, σ_σ.

$$\frac{\sigma_{x_Q}}{x_Q} = \left[1 - \frac{s_{BPM}}{L}\cot\frac{\sigma}{L}s_{BPM}\right]\frac{\sigma_\sigma}{\sigma} + \frac{\sigma_m}{m} \qquad (4.6)$$

In this case, error σ_m encompasses to statistical and systematic noise, as well as systematic calibration errors, related to the collection and processing of BPM data.
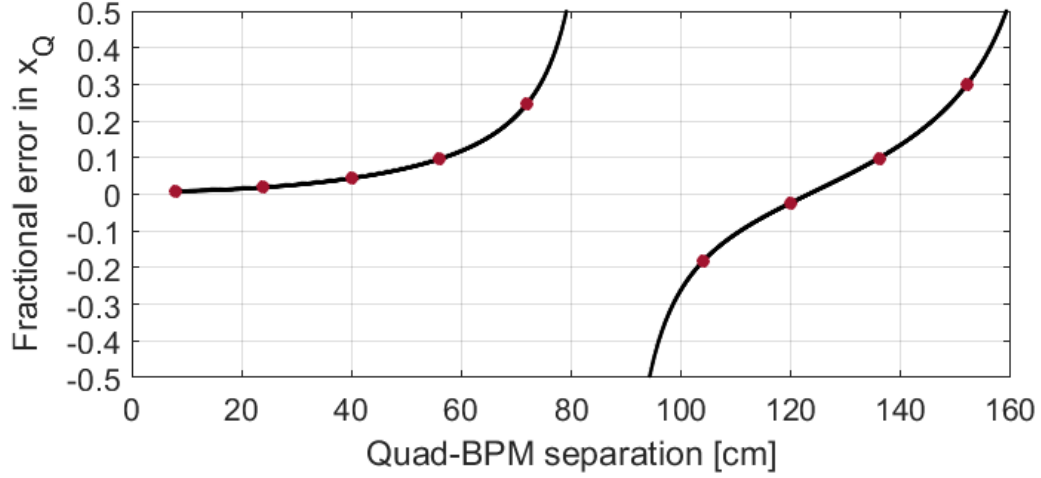
Fig. 4.6: Fractional error in quad-as-BPM position due to phase error, versus
quad and BPM separation

For all the data shown here, σ_m was taken to be the 90% confidence bounds of the
slope for the linear fit to the measured BPM position versus quadrupole strength
curve. This encompasses shot-to-shot noise and nonlinearities introduced by beam
scraping. Additionally, background was subtracted from scope traces to reduce the
effect of systematic, repeatable noise picked up by the BPM amplifiers.

σ_σ is an error introduced by using the VRUMER model to calibrate quadrupole
response data, and can be reduced by tweaking the focusing strength in the model.

Fig. 4.6 shows the dependence of the fractional error of measured position
in the quadrupole, x_Q, as a function of separation between quadrupole and BPM
used to measure quadrupole response. In this case, σ_σ is taken to be the systematic
error in phase advance between the VRUMER model and UMER experiment, $\sigma_\sigma = |$
$\sigma_{sim} - \sigma_{exp} | = 0.06$. Only 8 discrete quad-BPM separations exist, in the range
$[8, 24, 40, ...120]$ cm.

Tab. 4.2: "Next-downstream" Quad-BPM pairs with separations near half of a betatron wavelength, which results in large errors in the quad-as-BPM method.

Quad #	Nearest BPM
QR14	RC5
QR38	RC11
QR62	RC17
QR70	RC1 (turn 2)

As seen from Eq. 4.6, the error approaches ∞ where $\frac{\sigma}{L} s_{BPM} = n\pi$. This is the point where the betatron wavelength is equal to the quad-BPM separation, a null point of the perturbed orbit $\delta x(s) = x_Q \frac{L}{\sigma} \frac{G\Delta I}{B\rho} \sin \frac{\sigma}{L} s$. Near this null, the returned quad-as-BPM measurement will have large errors, and in general be very sensitive to error in the BPM measurement as well as differences in the model and experiment.

In standard UMER operation, the BPM spacing is 64 cm (see Fig. 4.5), and the associated error is maximum 10%. However, 4 BPM's are omitted for injection, longitudinal focusing and the wall current monitor. Larger errors are permitted at larger separations. Table 4.2) shows quadrupole-BPM pairs with fractional error > 1. The spacing for these 4 pairs is 88 cm, close to half the betatron wavelength, $\frac{\lambda}{2} \approx 86cm$.

In subsequent data shown, the 4 quads identified in Table 4.2 use the response measured in the next downstream BPM in order to avoid artificial blow-up or suppression of measured x_Q and y_Q.

4.6   Steering Algorithms

4.6.1   Horizontal Steering Algorithm

Horizontal orbit in the ring is controlled by 35 ring dipoles and the pulsed injection magnet (PD), for a ratio of 1 corrector per 2 quads. As the ring dipoles are designed to bend the beam 10°, they are sufficient to correct the background Earth field, which on average bends the beam $\approx 2.1^o$ per cell.

I applied VRUMER simulation to determine an effective algorithm for minimizing first turn orbit position in the quadrupoles by setting the 36 dipoles. As there are 2 quadrupoles per dipole, there are a variety of minimization functions available (aim for the center of either quadrupole, or some weighted combination of the two). I only considered quadrupoles immediately downstream of a given dipole, upstream of the next dipole. In these cases, multiple passes would be necessary to find a "centered" orbit, and relaxation is slow. The 2 downstream quadrupoles are indicated as focusing "F" or defocusing "D" based on polarity in the horizontal plane. The nearest downstream quadrupole for any dipole is focusing (in the standard FODO configuration), an sketched in Fig. 4.3.

I considered steering algorithms with an angle term x'. In the thin lens approximation for a focusing dipole separated from a defocusing dipole by a drift of distance L, $x'_F \equiv \frac{x_D - x_F}{L}$. I used $x'_F \propto x_D - x_F$ to include x'_F in the RMS minimization term, see Table **??**.

The results of multiple steering algorithms are shown in Table 4.3. Simulated

Tab. 4.3: Different algorithms and their performance (RMS position in quads) for initial condition $x = 1$mm, $x' = 0$.

shorthand	Minimization function	RMS(x_Q) [mm] no misalign.	RMS(x_Q) [mm] $\sigma = 5$mm	plot trace
x_F	$\lVert x_F \rVert$	5.3	37.3	○
x_D	$\lVert x_D \rVert$	0.2	6.9	△
x_F, x_D	$\sqrt{x_F^2 + x_D^2}$	2.1	9.3	◇
x_F, x_F'	$\sqrt{x_F^2 + (x_D - x_F)^2}$	0.2	6.6	*
x_D, x_F'	$\sqrt{x_D^2 + (x_D - x_F)^2}$	0.2	7.0	+

orbits with and without misalignment errors are shown in Fig. 4.7. Qualitatively, the best performers were x_D, x_F, x_F', x_D, x_F', resulting in almost identical orbits (sub-millimeter differences) that converge very quickly towards the center of the quads given an injection error or quad misalignment.

In the lab, it is much faster to minimize x_D, as the data collection is faster. It also allows interpolation between scanned dipole settings, as the data can be fit to a line and the zero-crossing calculated (the RMS minimization functions do not lend themselves to fitting by a simple function). However, when applied in the lab, the x_F, x_F' algorithm seems to yield better results. This may be because of its ability to handle relative misalignments between the focusing and defocusing quadrupoles, as well as reduced sensitivity to nonlinearities in the quad fields and BPM response for large centroid positions. For implementation in the lab (described in Section 4.7), I
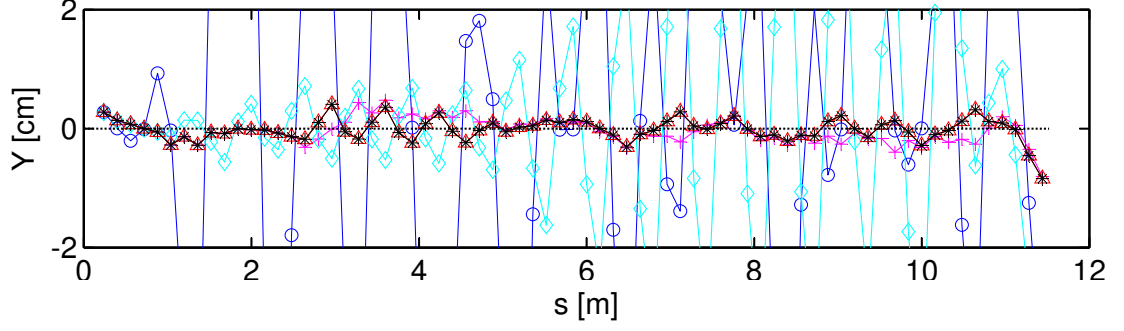
(a) No misalignments
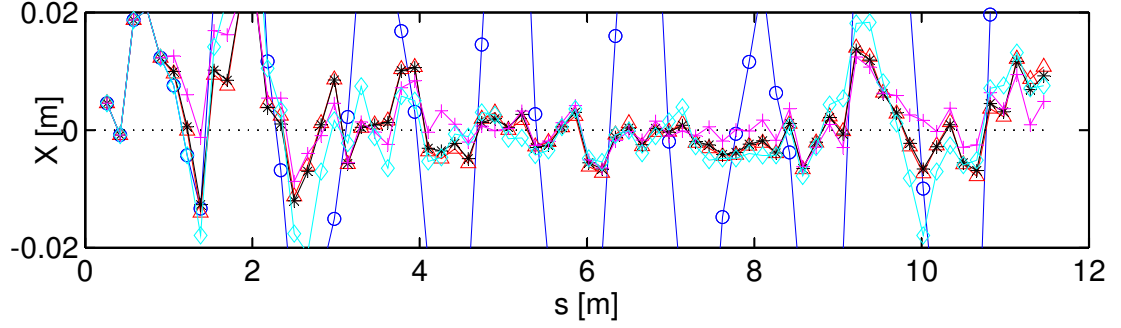
(b) Random quad misalignments from Gaussian distribution, $\sigma = 5$mm

Fig. 4.7: First turn VRUMER orbits for initial condition $x = 1$mm, $x' = 0$.

chose to use x_D as the minimization function, due to faster steering time.

4.6.2 Vertical Steering Algorithm

Vertical steering in UMER is accomplished by 18 vertical correction magnets (RSV's) located at the pipe flanges every 20°. All of these magnets are fairly weak (see Table 4.1) and spaced half as densely as horizontal correctors. The largest source of vertical alignment errors is the radial component of the Earth's field, shown in Fig. 4.1. Although the amplitude 200 mG is comparable to the vertical field, the average is only < 1 mG.
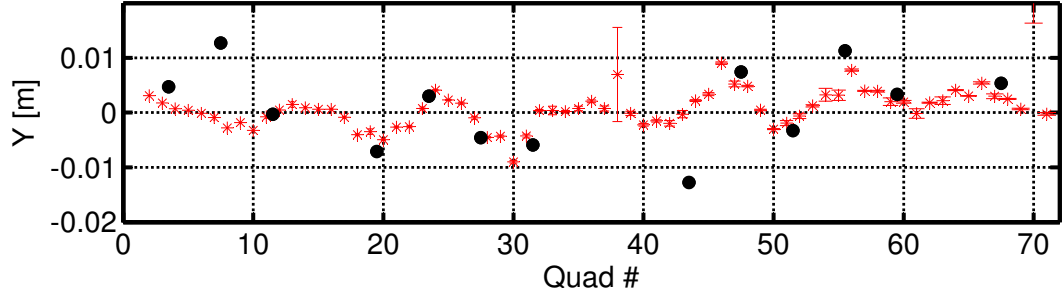
(a) Vertical position of 6 mA beam in quads for 1st turn.
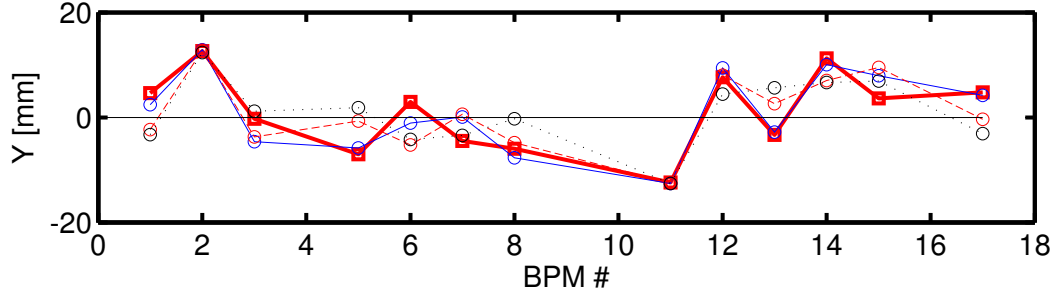
(b) Vertical position of 6 mA beam in BPMs for first 4 turns. Note shorted vertical plates at RC2, RC11.

Previous assumption has been that sparsely populated, low-field vertical correctors were sufficient to correct for the low average radial field. However, at regions of locally high radial field, the radial field bends $\approx 2.1^o$ per 2 ring cells, while the corrector at maximum safe excitation (determined by heat damage) of 2 A can only supply 1.2^o of correction. This results in locally high vertical excursions, as seen in Fig. 4.8a and Fig. 4.8b. In the first turn, the maximum vertical displacement from quad center is 10 mm and the RMS displacement is 3.2 mm.

While good recirculation is possible using the existing correctors, an attempt to steer through the vertical center of the quads will inherently be limited by the strength and density of vertical correctors. I use VRUMER to test various vertical

steering algorithms and place a lower bound on the best possible first turn orbit using existing vertical steerers, results are shown in Table 4.4. I considered three test cases:

- Ideal: Perfect alignment, RSV current constrained to be ≤ 10 A.

- SV limit: Perfect alignment, RSV current limited to ≤ 2 A.

- Misaligned: Random misalignment, from Gaussian distribution $\sigma = 1$ mm, RSV current limited to ≤ 2 A.

In summary, in the ideal case (strong correctors, no mechanical misalignments), we can obtain vertical steering with $\max(y) \sim 3$ mm, $\mathrm{rms}(y) \sim 1$ mm (Fig. 4.8a). This requires maximum RSV currents in the range 3-4 A, which is not possible given exiting heat dissipation limits. If we restrict ourselves to 2 A in the RSVs, the best possible solution is $\max(y) \sim 7$ mm, $\mathrm{rms}(y) \sim 2$ mm (Fig. 4.8b). Additionally, allowing for random vertical misalignments of order 1 mm, this increases to $\max(y) \sim 10$ mm, $\mathrm{rms}(y) \sim 3 - 4$ mm (Fig. 4.8c).

I conclude that the existing vertical correcters provide too weak of a correction to offer significant improvement on the existing first-turn solution. Enhanced vertical correction is necessary to achieve steering comparable to horizontal plane. This is possible through the use of radial field-cancelling Helmholtz coils or through addition of more weak vertical correctors (see Section 4.8).

Tab. 4.4: Vertical steering algorithms and their performance (RMS position in quads) for perfect alignment. Subscript indicates quad # counting downstream from vertical steerer (y_1 is position in first quad downstream from each RSV).

shorthand	Minimization Function	RMS(y_Q) [mm]	RMS(y_Q) [mm] SV limit	RMS(y_Q) [mm] $\sigma = 1\text{mm}$
SV=0	none	4.6	4.6	10.4
y_1	$\|y_1\|$	37.0		
y_3	$\|y_3\|$	1.5	2.2	3.8
y_4	$\|y_4\|$	1.7	2.5	3.4
y_1,y_2	$\sqrt{\frac{1}{2}\left(y_1^2 + y_2^2\right)}$	25.9		
y_2,y_3	$\sqrt{\frac{1}{2}\left(y_1^2 + y_3^2\right)}$	1.2	2.5	4.2
y_3,y_4	$\sqrt{\frac{1}{2}\left(y_3^2 + y_4^2\right)}$	0.98	2.4	3.7
y_1,y_3 (focusing)	$\sqrt{\frac{1}{2}\left(y_1^2 + y_3^2\right)}$	1.1	2.5	
y_2,y_4 (defocusing)	$\sqrt{\frac{1}{2}\left(y_2^2 + y_4^2\right)}$	0.93	2.6	4.6
y_1,y_1'	$\sqrt{\frac{1}{2}\left(y_1^2 + (y_2 - y_1)^2\right)}$	18.7		
y_2,y_2'	$\sqrt{\frac{1}{2}\left(y_2^2 + (y_3 - y_2)^2\right)}$	1.1	2.2	
y_3,y_3'	$\sqrt{\frac{1}{2}\left(y_2^2 + (y_4 - y_3)^2\right)}$	1.3	2.2	
y_1,y_2,y_3,y_4	$\sqrt{\frac{1}{4}\left(y_1^2 + y_2^2 + y_3^2 + y_4^2\right)}$	0.95	2.4	5.0
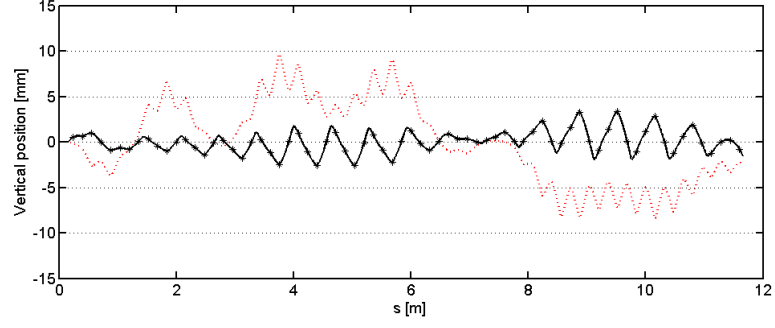
(a) Vertical steering for perfect alignment, no current limit. Steering by minimizing $\|y_4\|$. Red dotted trace is vertical solution without steering corrections.
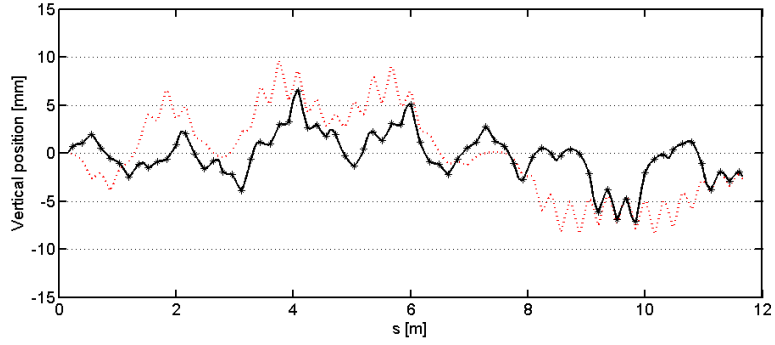
(b) Vertical steering for perfect alignment, RSV current limited to 2 A.
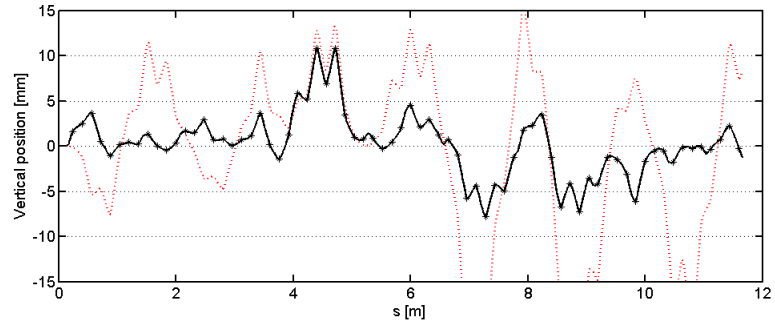
(c) Vertical steering for misalignment of $\sigma = 1$ mm, RSV current limited to 2 A.

4.7   Implementation

4.7.1   Quad-as-BPM position measurement

The process for collecting quadrupole reponse data and converting to quadrupole position data has been automated and stream-lined into the UMER control system. The procedure is conceptually straightforward. For a specified quadrupole, the algorithm:

1. Grabs a list of functioning BPM's, chooses downstream BPM for measurement of quad response (excluding pairs listed in Table 4.2).

2. Varies quadrupole over a preset range of ± 0.09 A around nominal set-point, using 5 data points total to calculate response.

3. Calculates response slopes $\frac{\Delta X_{BPM}}{\Delta I_{quad}}$ and $\frac{\Delta Y_{BPM}}{\Delta I_{quad}}$ by applying linear least squares fit to response data.

4. Runs VRUMER simulation 9 times to calculate simulated response slope for given quad-BPM pair. Divide x_q, y_q by response slope to determine slope-to-position calibration factor.

5. Applies VRUMER calibration factor to measured response slope to return measured position in quad.

6. Calculates error to response slope, including 95% confidence interval to slope, as well as quad-BPM separation relation to phase advance, according to Eq. 4.6.

Arguably, the slope-to-position calibration factor could be generated using a matrix-based tracking technique (as outlined in [**?**]) and saved as a look-up table. For a given quad-BPM separation (for 72 quadrupoles there are only 8 possible separations), this number is not expected to change much and this approach would require fewer computations. However, this comes with an added loss of flexibility. The look-up table would have to be recalculated for UMER operating points with different quad focusing strengths or non-FODO orientations. For example, Chapter **??** uses an alternative lattice configuration with half the quads turned off. The time savings for using a look-up table are small. Running VRUMER takes ~ 0.06 seconds, so even for the an entire quad scan (9 points) VRUMER costs ~ 0.5 second per quad. This is negligible compared to the time required to measure BPM response for multiple quad settings.

There is a slight discrepancy with the phase-advance contribution to error bar calculation. The error $\sigma_\sigma \equiv |\sigma_{exp} - \sigma_{sim}|$. Simulated phase advance σ_{sim} is estimated from VRUMER results using NAFF algorithm [4], [5]. Experimental phase advance σ_{exp} is hard-coded to be $\nu_x = 6.636$, $\nu_y = 6.752$ for standard 1.826 A operating point. This will result in erroneaously large error bars for different operating points and should be modified in the future to be more general.

4.7.2   Steering Procedure

This is a description of the horizontal steering method I used to steer the 6 mA beam on November, 2015. The final solution was saved as settings file kiersten_6mA_151116.csv.

The procedure for horizontal steering attempts to steer the beam as close as possible to the center of the quads in the first turn, and use two dipoles at the end of the ring to close the orbit. I generated this solution using an existing solution with many turns, but it should be possible to apply this method to a ring with "no-steering" (significant current loss in the first few turns). The procedure is as follows:

1. Set last 2 injection dipoles by scanning currents and identifying smallest rms deviation in first two RQ's after injection. Time: 1 hour.

2. Steer through RQ3 (first turn) by setting current in D1; Repeat injection scan if change was significant. Time: 10 minutes + 1 hour if repeating injection scan.

3. Steer through quads in first turn, setting dipoles D2-34 in order and using quad-as-BPM method to measure position in quads. Time: 2 1/2 hours ($\times 2$ for best results).

4. Close orbit by scanning D34 and D35 currents. Time: 30 minutes

5. Verify orbit quality by running quad scan for 1st turn quad-as-BPM data, and look at multi-turn BPM data to estimate orbit excursions from closed orbit. Time: 30 minutes.

Total (minimum) time for steering: ≈ 6 hours. Time estimates are for total measurement/ beam-on time, more time should be added for trouble-shooting and general unruly behavior.

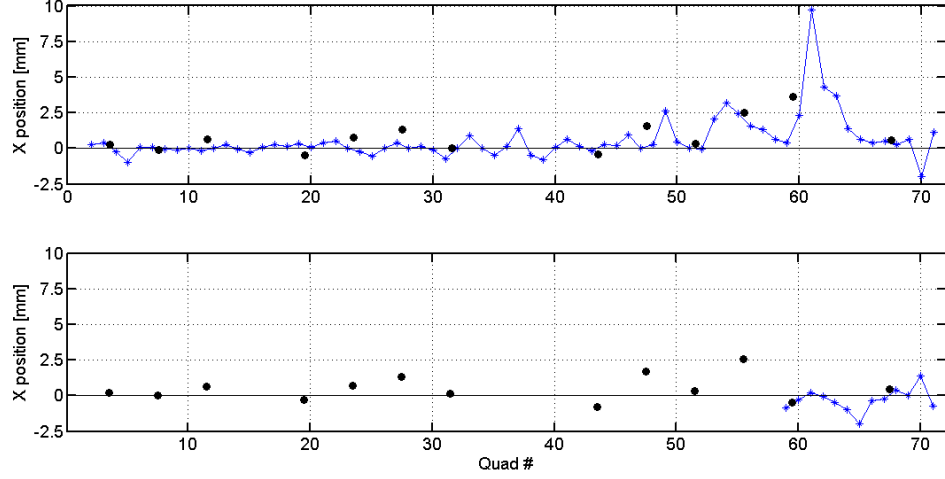*Fig. 4.8:* 1st turn solution generated on 11/13/15 (top) and 11/16/15 (bottom), by steer-

ing through defocusing quadrupoles.

Points Rejection

A weakness of the $\|x_D\|$ minimization is that occasionally the data will not

fall on a straight line. This is most likely due to scraping between the dipole and

BPM or noise in the region near the pulser. In the ring steering scripts, I have

implemented a points rejection critera that throws away quad position data with

errorbar > 1 mm. As the errors is proportional to the uncertainty in the fitted

slope of the quad response, large non-linearities in the quad response will manifest

as large error bars. This is typical of large centroid excursion in either the quad or
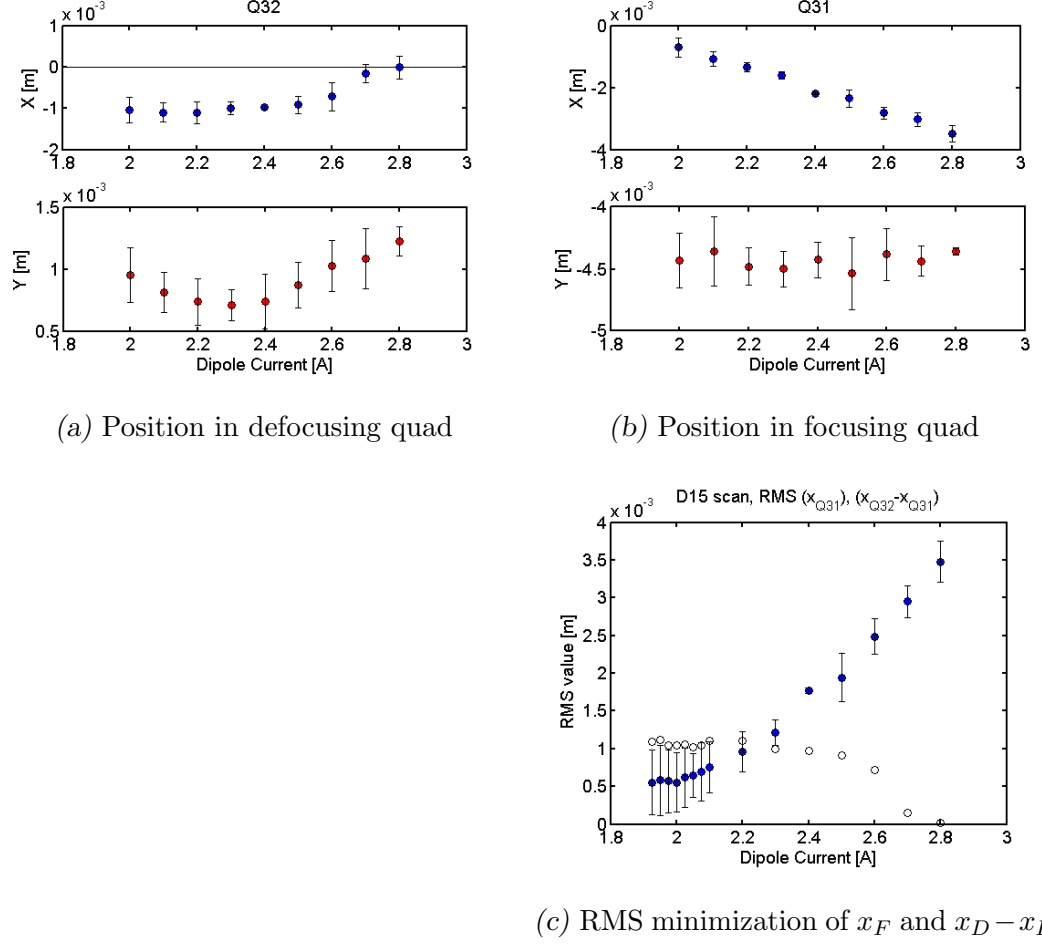
the BPM.

(a) Position in defocusing quad   *(b)* Position in focusing quad

(c) RMS minimization of x_F and $x_D - x_F$

Fig. 4.9: Steering through D15 using two different algorithms, 11/11/15

Closing the orbit

The final step is to set the current in the dipoles near the end of the ring so that the closed orbit is close to the p1 closed orbit. Two dipoles are required for control of x and x'. Naively, one would vary the last two dipoles, D35 and PD-Rec. Unfortunately PD-Rec has significant coupling with the first turn beam position. For a scan of PD-Rec from 8.25 → 13.75 A, the position of the beam in the first BPM varies in the range $\Delta x = \pm 2$mm. Changing PD-Rec would mean changing all

ring dipole settings to compensate, which is undesirable.

It is possible but difficult to optimize the value of PD-Rec. Instead, I assume that the present setting (PD-Rec I= 11 A) is reasonably close to the ideal value such that closing the orbit with D34 and D35 will result in a bump in the closed orbit in that neighborhood. It may be possible to infer, based on the difference in the D34 currents optimized for a) steering through RQ69 and RQ70 and b) a closed orbit solution, the size of the orbit bump.

To set D34 and D35, I scan the currents in each and record the BPM response for the first four turns in the first 3 BPMs. I try to minimize the RMS change in position between turn 1 and turn $N \leq 4$ in the first three BPM's. For each BPM 1-3, I define an RMS quantity $\sqrt{\frac{1}{3}\left[(x_2 - x_1)^2 + (x_3 - x_1)^2 + (x_4 - x_1)^2\right]}$. In order to find a good closed orbit, I ran 3 scans, increasing the resolution and/or re-centering the scan range for each successive scan. Scan takes $\sim$13 minutes to read 3 BPMs for 11 current settings in each dipole.

4.8   Increasing Vertical Steering Capability

4.9   Comments on steering the Alternative Lattice

4.10   Global Optimization of Closed Orbit
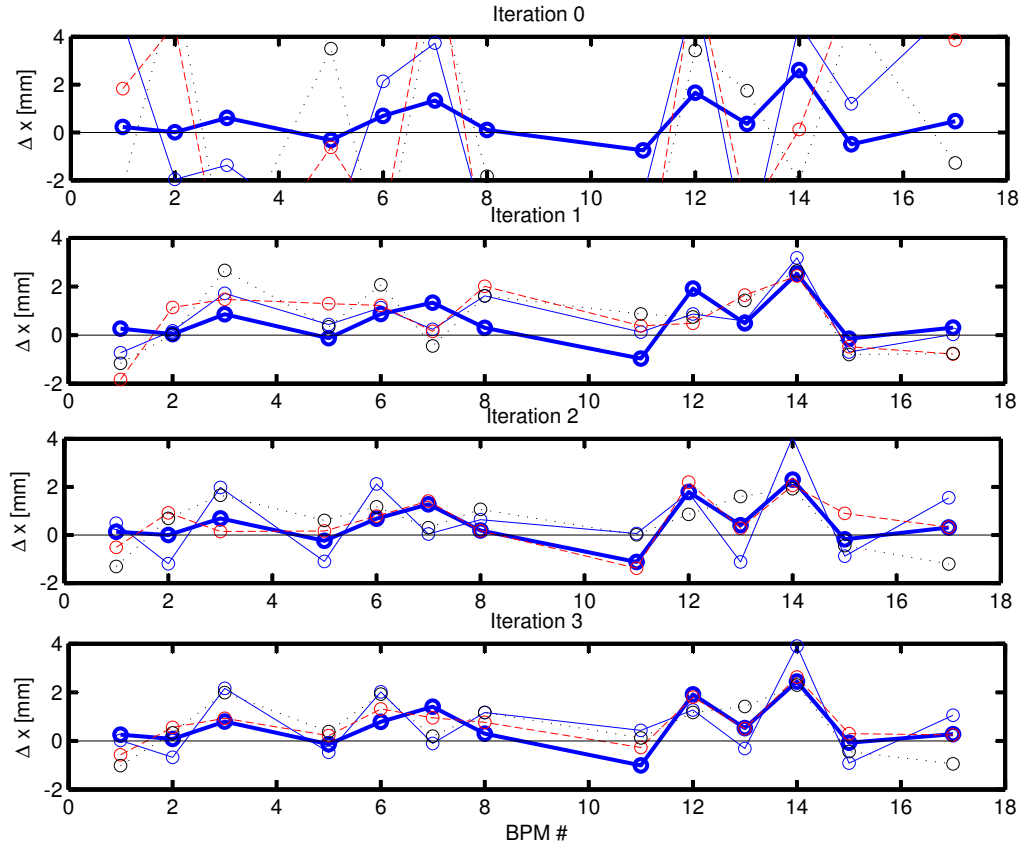
[6] [7], [8]

Fig. 4.10: BPM response for first 4 turns, for D34, D35 currents listed in table **??**. 1st turn: heavy blue trace. 2nd turn: solid blue. 3rd turn: long dash red. 4th turn: short dash black.
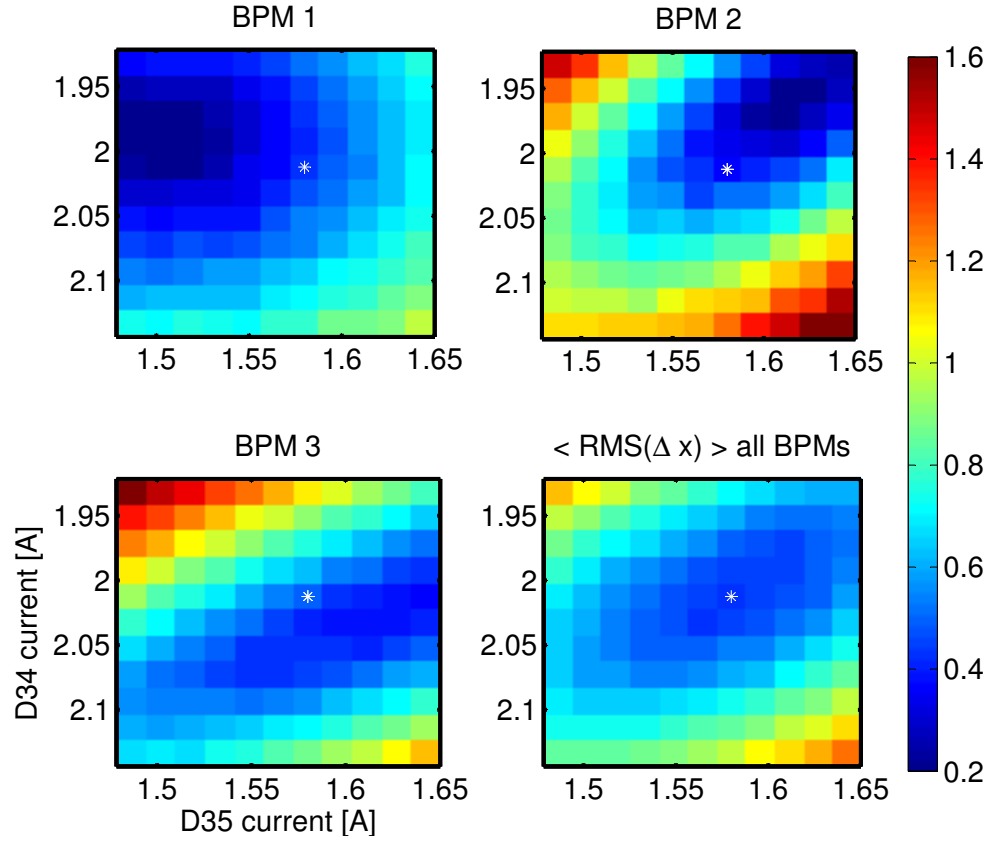
Fig. 4.11: Scan results for first 3 BPMs for iteration 3 in table **??**. Color scale is rms value of Δx over first 4 turns [mm], white asterisk indicates optimal setting (D34=2.0129 A, D35=1.5802 A)

Bibliography

[1] K PoorRezaei. Measurement of closed orbit reponse matrix for umer. Technical report, University of Maryland, IREAP, Dec 2011.

[2] K PoorRezaei. Measuring beam centroid position inside quadrupoles. Technical report, University of Maryland, IREAP, March 2012.

[3] R Kishek. First principles tune calculation for umer. Technical report, University of Maryland, IREAP, May 2010.

[4] J. Laskar. Frequency map analysis and particle accelerators. *Particle Accelerator Conference, Portland*, 1(2), 2003.

[5] Kevin Pedro. Frequency Mapping Analysis for Nonlinear Dynamics in Particle Accelerators. pages 1–12, 2012.

[6] Author S Kirkpatrick, C D Gelatt, and M P Vecchi. Optimization by Simulated Annealing. *Science*, 220(4598):671–680, 2015.

[7] Xiaobiao Huang, Jeff Corbett, James Safranek, and Juhao Wu. An algorithm for online optimization of accelerators. *Nuclear Instruments and Methods in Physics Research, Section A: Accelerators, Spectrometers, Detectors and Associated Equipment*, 726:77–83, 2013.

[8] L. Dovlatyan. private communication, 2017.